


Application of an Incomplete Landslide Inventory and One Class Classifier to Earthquake-Induced Landslide Susceptibility Mapping

Shuai Chen, Zelang Miao , Member, IEEE, Lixin Wu, and Yueguang He

Abstract—Rapid and effective evaluation of landslide susceptibility after earthquakes is critical for various applications, such as emergency rescue, land planning, and disaster prevention. Current research suffers from the lack of a complete landslide inventory and sample selection uncertainty issues. To solve these problems, this study presents a landslide susceptibility mapping model that integrates one-class support vector machine (OCSVM) and an incomplete landslide inventory, which was established with the aid of change detection from bi-temporal Landsat images. Wenchuan County is selected as the study area to test the performance of the proposed method. The proposed method is also compared with standard two-class SVM that selects a sample randomly. Experimental results show that OCSVM can achieve better performance than SVM when only an incomplete landslide inventory is available. The findings of this study can be applied to determine regional landslide susceptibility after earthquakes and provide an essential reference for emergency response.

Index Terms—Earthquake-induced landslide, incomplete landslide inventory, landslide susceptibility, one-class support vector machine, slope unit.

I. INTRODUCTION

ON May 12, 2008, a MS 8.0 earthquake occurred in Wenchuan county, Sichuan province, which triggered a large number of landslide, causing great economic losses and casualties [1]. In the process of post-earthquake emergency rescue, it is necessary to quickly locate the high-risk area of seismic landslide, so as to provide a basis for seeking the best rescue opportunity and optimizing emergency rescue deployment. Although remote sensing technology can quickly obtain

Manuscript received January 8, 2020; revised February 26, 2020; accepted March 30, 2020. Date of publication April 13, 2020; date of current version May 4, 2020. This work was supported in part by the National Key R&D Program of China under Grant 2018YFC15035, in part by National Natural Science Foundation of China under Grant 41701500 and Grant 41930108, in part by the Natural Science Foundation of Hunan Province under Grant 2018JJ3641 and Grant 2019JJ60001, in part by Talents Gathering Program of Hunan Province under Grant 2018RS3013, in part by Innovation-Driven Project of Central South University under Grant 2020CX036, and in part by Early-Stage Research Start-up Grants funded by Central South University under Grant 502045001 and Grant 506030101. (Corresponding author: Zelang Miao.)

Shuai Chen, Zelang Miao, and Lixin Wu are with the School of Geoscience and Info-Physics and Key Laboratory of Metallogenic Prediction of Nonferrous Metals and Geological Environment Monitoring, Ministry of Education, Central South University, Changsha 410083, China (e-mail: chens1227@163.com; zelang.miao@outlook.com; awulixin@263.net).

Yueguang He is with the School of Traffic and Transportation Engineering, Changsha University of Science and Technology, Changsha 410004, China (e-mail: 894077350@qq.com).

Digital Object Identifier 10.1109/JSTARS.2020.2985088

post-earthquake high-resolution image and obtain the actual landslide distribution, it is difficult for traditional technology to identify potential susceptibility areas under earthquake disturbance. Therefore, timely evaluation of landslide susceptibility after an earthquake is critical to various applications, such as emergency rescue and disaster prevention [2].

Susceptibility models of seismic landslides can be divided into two categories, namely, Newmark displacement and statistical analysis methods. The method of Newmark displacement analysis combines the slope stability before an earthquake and seismic wave disturbances to evaluate landslide susceptibility. This method has attracted considerable attention from researchers due to its simple mechanical principle. For example, the method has been applied to analyze the 1994 Mw6.7 Northridge earthquake [3], the 1997 M4.4 Umbria Marche earthquake [4], the 1999 M_l = 7.3 Chi-Chi earthquake [5], [6], the 2008 Mw8.0 Wenchuan earthquake [7], the 2013 Mw7.0 Lushan earthquake [8], [9], the 2015 Nepal earthquake [10], the 2016 Kumamoto earthquake [11], and the 2017 Jiuzhaigou earthquake [12]. However, the prediction of the Newmark model requires detailed and accurate geotechnical parameters and ground motion parameters to calculate the displacement of the slope, which is often difficult to obtain under current technical conditions [13]. Therefore, landslide susceptibility mapping based on the Newmark model alone is still challenging.

The statistical analysis method uses landslide inventories to establish a statistical model of a landslide and its influence factors. Typical statistical models include an index of entropy (IoE), analytic hierarchy process (AHP), weight of evidence (WoE), artificial neural networks (ANN), support vector machine (SVM), logistic regression (LR), and random forest (RF). For example, Yi *et al.* [14] used AHP to produce a landslide susceptibility map of Jiuzhaigou in Sichuan Province, China. Mondal and Mandal [15] utilized the IoE model to map the landslide susceptibility zones of Darjeeling Himalaya, India. Kayastha *et al.* [16] applied the WoE model to analyze landslide susceptibility in Tinau Watershed, Nepal. Xu *et al.* [17] used the LR model to obtain a landslide susceptibility map in China. Shahri *et al.* [18] adopted and verified landslide susceptibility results obtained using ANN, and GIS was applied to southwest Sweden. The SVM model was also used to produce reliable susceptibility maps in China [19] and Iran [20].

With the widespread application of numerous models, model performance has attracted increasing attention. For instance, Kim *et al.* [21] used RF and boot tree (BT) to produce and compare two landslide susceptibility maps in Korea; they found that the BT model is better than the RF model. Pradhan [22] compared the predictive ability of decision tree (DT), SVM, and adaptive neuro-fuzzy inference system (ANFIS) in landslide susceptibility mapping using GIS. The results showed that the use of the three models in Malaysia is viable. Pham *et al.* [23] compared and analyzed the performance of different models (e.g., SVM, LR, BN, NB, and FLDA) in landslide susceptibility mapping and found that the SVM model exhibits the best performance among all of the compared models. Meanwhile, Hong *et al.* [24] used four different kernel functions in the SVM model to predict the spatial distribution of landslides triggered by the Yushu earthquake. Their results showed that the RBF-SVM model has the highest overall performance. More about statistical analysis method can reference to the review article [2]. Different from the Newmark displacement analysis method, the statistical analysis method does not require detailed and accurate geotechnical parameters. The statistical model is built based on the distribution information of real earthquake-induced landslides, and the results are more objective by taking the effect of complex geological environment impact factors into comprehensive consideration.

Sample selection is necessary for building a statistical model of landslide susceptibility. The following methods can be used in the selection of a non-landslide sample: (1) random selection in a landslide-free area [19], [23], [25], (2) random selection in areas beyond the landslide buffer distance [17], and (3) random selection in an extremely low susceptibility area by building an initial susceptibility map [26]. These sample selection methods assume that complete landslide inventories are available, that is, the area outside the landslide is the landslide-free area. Therefore, the statistical analysis method relies on the quality of input landslide inventories, which greatly limits the practical application of landslide susceptibility.

Landslide inventories are key to study the distribution of landslides, to assess the main mechanisms of slope failure, and to generate landslide hazard maps. With the development of remote sensing, especially the availability of optical image, it is possible to obtain complete landslide inventory after the earthquake. For reliable landslide inventories, most existing studies still exploit time-consuming and labor-intensive visual interpretation in practical applications [1], [27], [28]. However, this approach has difficulty in meeting rapid emergency needs. Compared with visual interpretation, semi-automatic interpretation can realize rapid landslide inventory mapping for a large area. Common methods include change detection [29]–[31], pixel-based analysis [32] and object-based analysis [33], [34]. However, the existing semi-automatic interpretation still have many shortcomings in practical applications, such as misclassification of areas, over prediction of landslide areas, and difficult to separate amalgamated landslide zones. On the other hand, as the main data source of landslide inventory mapping, the quality of optical image is also an important factor. For earthquake events, the earthquake is often accompanied by severe weather conditions,

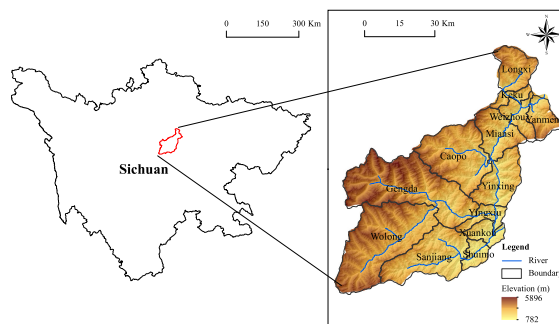


Fig. 1. Geographical location of the study area.

post-earthquake areas are covered by clouds; it is difficult to obtain cloud-free images. For earthquake events, earthquakes are often accompanied by severe weather conditions, and the area after the earthquake is covered by clouds, making it difficult to obtain cloud-free images, which also affects the complete of the landslide inventories. Therefore, how to carry out landslide susceptibility evaluation based on an incomplete landslide inventories and provide data support for post-earthquake emergency rescue work.

In response to these problems, this study used an incomplete landslide inventory to build a landslide susceptibility model on the basis of one-class SVM (OCSVM). Different from the traditional statistical model, OCSVM only needs single-type sample data, which can better deal with the uncertainty of the traditional statistical model on the selection of non-landslide samples and reduce the dependence on the complete landslide inventories. Wenchuan County, which was struck severely by an earthquake in 2008, was used as the study area. The reliability of the model was verified and analyzed through complete landslide inventories and new landslide events. This work can provide a reference for post-earthquake emergency rescue, land use planning, and disaster prevention.

II. STUDY AREA AND DATA SOURCES

A. Study Area

The study area, which is located in Wenchuan County of Sichuan Province, was severely affected by the Wenchuan earthquake last May 12, 2008. The area is dominated by high mountainous terrain with significant fluctuation, and it has a relative elevation of 782–5896 m. Affected by complex geological and topographical conditions, the 5.12 Wenchuan earthquake triggered numerous landslides and caused substantial property losses and casualties in the disaster area. Fig. 1 presents the geographical location of the study area.

B. Data Sources

The data sources used in this work included six parts. (1) The initial landslide inventory was obtained quickly by using the change detection (CD) of pre- and post-earthquake Landsat-7 ETM+ (Imaging dates: April 22, 2008 and May 25, 2008). Influenced by climate, technology, and other factors, the initial landslide inventory was defined as an incomplete landslide

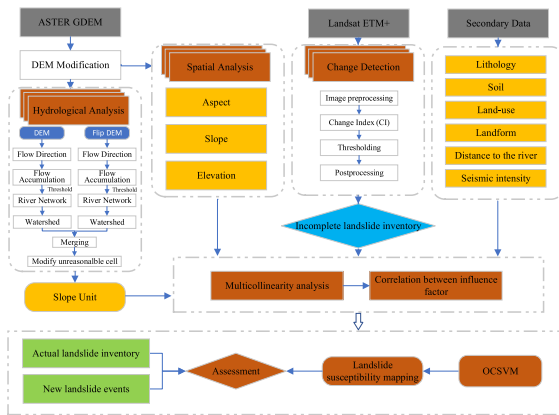


Fig. 2. Flowchart of the landslide susceptibility map based on OCSVM.

inventory and mainly used to build the model of landslide susceptibility. (2) The complete landslide inventory was acquired from Xu *et al.* [1]; it was obtained via visual interpretation and field investigation using pre- and post-earthquake multi-source high-resolution remote sensing images (e.g., CBERS-02B, IRS-P5, ASTER, ALOS, SPOT 5, IKONOS, and QuickBird). This inventory was used to verify the results of landslide susceptibility. (3) A DEM with a spatial resolution of 30×30 m was derived from the data of Advanced Spaceborne Thermal Emission and Reflection Radiometer Global Digital Elevation Model¹ and mainly used to obtain the slope, aspect, elevation, and other landslide influence factors. (4) A geological map of the study area was obtained from the Geological Bureau of China. (5) A seismic intensity map of the study area was acquired from the China Seismological Bureau² and mainly used to obtain seismic influence factors. (6) Other data (e.g., land use, landform, and soil) were obtained from the Resource and Environment Science Data Center of the Chinese Academy of Sciences³ and used to collect other landslide influence factors.

III. METHODOLOGY

Remote sensing images have been widely used in seismic disaster extraction because of their broad coverage and convenient data acquisition. However, due to the influence of cloud and fog, obtaining a complete seismic landslide distribution after an earthquake is difficult. On the basis of remote sensing images, we can rapidly obtain an incomplete landslide inventory, construct a landslide susceptibility model, and determine the regional distribution of landslide susceptibility. The flowchart of the proposed method is shown in Fig. 2.

A. Acquisition of an Incomplete Landslide Inventory

A complete landslide inventory provides primary data for the evaluation of regional landslide susceptibility. Visual interpretation is the main method for the acquisition of a landslide inventory, and a considerable amount of time and manpower are

¹Online. [Available]: <https://gdex.cr.usgs.gov/gdex/>

²Online. [Available]: <https://www.cea.gov.cn/>

³Online. [Available]: <http://www.resdc.cn/Default.aspx>

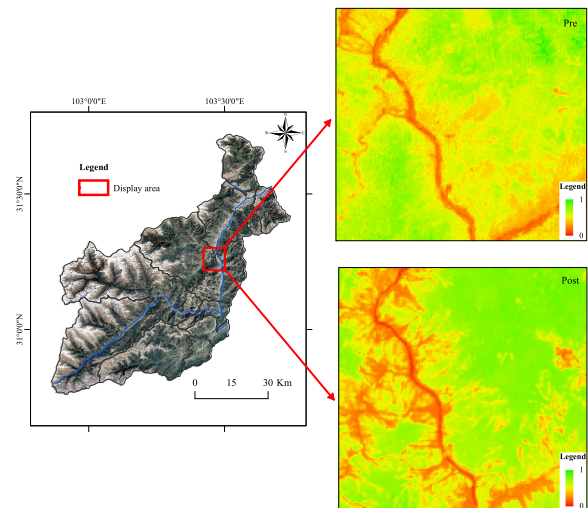


Fig. 3. Pre- and post-earthquake NDVI distribution.

needed in a large area. However, this approach has difficulty in meeting rapid emergency needs. Compared with visual interpretation, semi-automatic extraction technology, especially change detection, can quickly obtain landslide inventories through remote sensing images pre- and post-earthquake [29], [30], [35]. However, due to uncertain factors, such as cloud, fog, and terrain effects, it is difficult to obtain detailed complete landslide inventory.

A landslide destroys vegetation on the ground during formation and sliding, resulting in low or no vegetation coverage. The near-infrared (NIR) band has strong reflection characteristics in a vegetation coverage area, and the visible light band has strong absorption characteristics. A vegetation index for a quantitative analysis of vegetation coverage can be constructed through the spectral differences between visible and NIR regions of vegetation. NDVI is sensitive to the change of surface vegetation and has been widely used in landslide extraction [36], [37]. Therefore, in this study, the change detection based on NDVI was used to product landslide inventory.

For change detection, image preprocessing is an essential preparation. It mainly includes image correction, radiation correction, atmospheric correction, and cloud mask processing. Then, pre- and post-earthquake NDVIs were constructed using Eq. (1), as shown in Fig. 3, by using NIR and red band (R) spectral information. This figure indicates that the NDVI of the landslide after the earthquake was lower than that before the earthquake; this information can be used to identify the landslide.

$$NDVI = \frac{(NIR - R)}{(NIR + R)}. \quad (1)$$

To extract change information, the Change Index (CI) before and after the earthquake is obtained by using the image difference base on NDVI. More specifically, the value of the CI for a specific pixel is defined as $CI(i, j) = NDVI(i, j)^{pre} - NDVI(i, j)^{post}$, in which $NDVI(i, j)^{pre}$, and $NDVI(i, j)^{post}$ are pixel values obtained before and after earthquake, respectively. Usually, for the landslide area, the post-earthquake vegetation

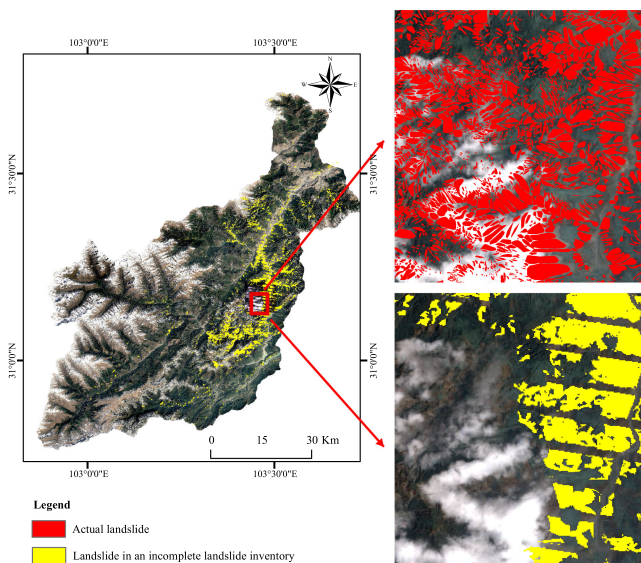


Fig. 4. Incomplete landslide inventory in Wenchuan County extracted by change detection.

is significantly less than that before the earthquake, showing a significant negative value on the CI, while the CI of other areas should be close to 0. Therefore, to extract the landslide area, the CI of each pixel is compared with a given threshold value. If the threshold value is less than or equal to the threshold value, it is labeled as landslide; Otherwise, it is marked as a background pixel. Specifically, the threshold can be obtained by comparing multiple groups of experiments. The threshold was set to -0.27 in this experiment. Finally, the results were post-processed as necessary, including morphological operations and manual removal of misclassification.

The landslides extracted by change detection are shown in Fig. 4. It can be seen that the change detection method can identify most large and medium-sized landslides, but there are obvious omissions in small landslides and cloud-covered areas. At the same time, affected by the image resolution, it is difficult to separate amalgamated landslide zones. By comparing the actual landslide distribution, it can be found that the landslide area extracted by change detection is 169.06 km^2 , far less than the actual landslide area of 359.22 km^2 , only 47% of the actual landslide area is extracted. Therefore, the landslide inventories are incomplete.

B. Mapping Unit and Landslide Influence Factors

1) *Mapping Unit*: The mapping unit is a critical foundation of a landslide susceptibility model [2]. Existing research is mainly based on the grid unit, which is a regular independent mapping unit that is easy to realize and simple to calculate and has been widely used in the evaluation of landslide susceptibility [9], [18], [38]. However, the grid unit has difficulty expressing complex geological environment information, which entails many problems, such as large amounts of data and long calculation time [39]. Unlike the grid unit, slope units (SUs) correspond to geomorphic units and are bounded by drainage

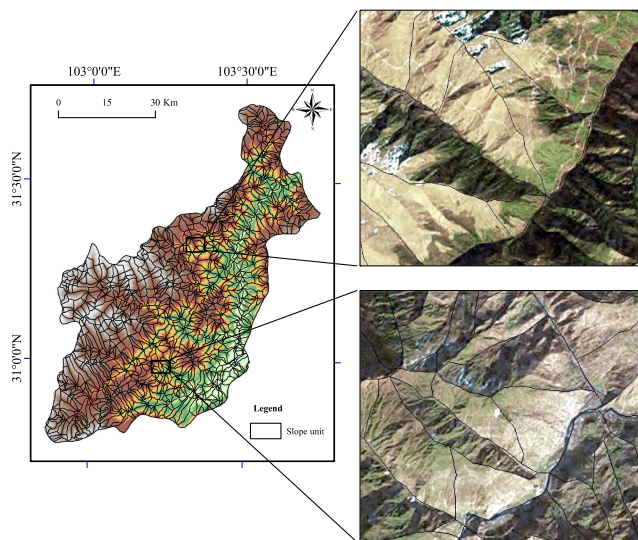


Fig. 5. SU of the study area.

and boundary lines; they can effectively reflect geomorphic and topographic information. A landslide is a geological disaster phenomenon developed on a slope. Therefore, research on landslide susceptibility based on SU can reliably reflect the degree of landslide susceptibility in disaster areas. In ArcGIS platform, SUs are extracted by DEM. A SU can be considered either as part of a slope or as half of a drainage basin, which can be divided into two SUs based on a ridgeline and a valley line. The flowchart of SU extraction is shown in Fig. 2. For the selection of flow threshold, the optimal parameters were determined according to the artificial multi-group experiment. In this experiment, 5000 was uniformly used as the flow threshold. Further details about the SU obtained can be found in the work of [36]. The study area was divided into 1351 SUs, as shown in Fig. 5.

2) *Landslide Influence Factors*: Seismic landslides are formed under the comprehensive action of various influence factors under complex geological conditions. Reasonable selection of influence factors is an essential prerequisite for the evaluation of landslide susceptibility [40]. Landslide influence factors can be typically divided into controlling and inducing factors. Controlling factors, such as geological sites and landforms, are static and essential in the original stability of the earthquake area. Inducing factors, such as heavy rainfall, earthquake, and human engineering activities, are dynamic and can promote or inhibit the occurrence of landslides. The formation of seismic landslides involves the comprehensive influence of controlling and inducing factors. Therefore, controlling factors, such as topography, geology, and hydrology, and inducing factors related to the earthquake were selected as the influence factors of the landslide in this study.

1) Seismic intensity refers to the ground shaking caused by an earthquake and the intensity of its impact is generally used to describe the damage caused by earthquakes in different regions. Seismic intensity is the main inducing factor of seismic landslides. Previous studies have shown that landslides are likely to occur in areas with

TABLE I
INFLUENCE FACTORS OF THE SEISMIC LANDSLIDE

Influence factors	Numbers	Value
Seismic intensity	4	1. XI; 2. X; 3. IX; 4. VIII
Distance to the river (km)	11	1. 00.5; 2. 0.51; 3. 11.5; 4. 1.52; 5. 22.5; 6. 2.53; 7. 33.5; 8. 3.54; 9. 44.5; 10. 4.55; 11. >5
Elevation (km)	10	1. 0.51; 2. 11.5; 3. 1.52; 4. 22.5; 5. 2.53; 6. 33.5; 7. 3.54; 8. 44.5; 9. 4.55; 10. >5
Slope (°)	8	1. 010; 2. 1020; 3. 2030; 4. 3040; 5. 4050; 6. 5060; 7. 6070; 8. >80
Aspect	9	1. Flat; 2. N; 3. NE; 4. E; 5. SE; 6. S; 7. SW; 8. W; 9. NW
Lithology	10	1. Sandstone; 2. Magmatic rock; 3. Phyllite; 4. Shale; 5. Glutnite; 6. Carbonate rock
Soil	5	1. Leached soil; 2. Semileached soil; 3. Primary soil; 4. Alpine soil; 5. Ferralsol; 6. Rock
Landform	7	1. Plain; 2. Platform; 3. Hill; 4. Small undulating mountain; 5. Middle undulating mountain; 6. High undulating mountain; 7. Very high undulating mountain
Land use	5	1. Cultivated land; 2. Woodland; 3. Grassland; 4. Water; 5. Urban and rural residents

high seismic intensity [41]. According to the seismic intensity provided by Sichuan Seismological Bureau, the study area contains four seismic intensity zones [Table I, Fig. 6(a)]. The main seismic intensity level of each SU was adopted as the corresponding seismic intensity attribute of the SU.

- 2) A river is a crucial factor that affects the occurrence of landslides. Erosion and cutting of rivers can weaken the stability of slopes [17]. In accordance with the river distribution of the study area, the buffer zone was established based on a distance of 0.5 km, and the study area was divided into 11 categories [Table I, Fig. 6(b)]. The value closest to the river in each SU was assigned the SU river attribute.
- 3) Elevation is closely related to the development and distribution of landslides. Elevation controls surface water runoff and affects seismic disturbance. In accordance with the DEM of the study area, elevation was divided based on a height difference of 0.5 km. The study area was divided into 10 categories [Table I, Fig. 6(c)]. The main elevation level in an SU was set as the elevation attribute of the SU.
- 4) Slope is crucial in the occurrence of landslides. The key to the formation of landslides lies in whether the slope has a valid free surface. The stress concentration under the action of an earthquake is likely to cause a landslide in an area with a steep slope. For the study area, DEM was used to obtain the slope distribution, and the slope was discretized based on a 10° interval, which was divided into eight categories [Table I, Fig. 6(d)]. The main slope grade in each SU was taken as the slope attribute of the SU.
- 5) Aspect is defined as the projection direction of the slope normal to the horizontal plane. Clear differences exist in the distribution of seismic landslides in a different aspect due to the influence of solar radiation and earthquake disturbance. In accordance with the value range of the aspect, the study area was divided into nine grades [Table I, Fig. 6(e)] with 45° as a zone. The main aspect information in each SU was taken as the aspect attribute of the SU.
- 6) Lithology is an essential component of a slope. Rock type determines the weathering strength and mechanical properties of rock and soil mass. Different lithologies are affected by seismic disturbance differently. According to the geological map, the study area contains 10 kinds of

TABLE II
CORRELATION COEFFICIENT BETWEEN INFLUENCE FACTORS

F1 ¹	F2	F3	F4	F5	F6	F7	F8	F9	
F1	1								
F2	0.43	1							
F3	-0.03	-0.13	1						
F4	0.66	0.26	-0.04	1					
F5	-0.03	-0.09	0.11	-0.15	1				
F6	0.49	0.19	-0.08	0.26	0.04	1			
F7	-0.02	0.00	0.15	0.00	0.02	-0.02	1		
F8	0.79	0.27	0.05	0.65	-0.01	0.41	0.02	1	
F9	-0.07	0.02	-0.09	-0.07	0.03	-0.04	0.06	-0.02	1

¹F1–F9 represent elevation, soil, slope, distance to the river, lithology, land use, seismic intensity, landform, and aspect, respectively.

lithology [Table I, Fig. 6(f)]. The main lithology in each SU was taken as the lithology attribute of the SU.

- 7) Soil is a critical component of a slope. According to the distribution of soil types provided by the data center of the Chinese Academy of Sciences, five soil types are mainly distributed in the study area [Table I, Fig. 6(g)]. The main soil types in each SU were taken as the soil attribute of the SU.
- 8) Landform can be divided into different types according to the differences in geomorphic genesis and morphology. According to the landform distribution provided by the data center of the Chinese Academy of Sciences, seven landforms are mainly distributed in the study area [Table I, Fig. 6(h)]. The main landform in each SU was regarded as the landform attribute of the SU.
- 9) Land use is a land attribute with different purposes and characteristics formed in the process of human activities. According to the land use distribution provided by the data center of the Chinese Academy of Sciences, the study area mainly includes five land-use types [Table I, Fig. 6(i)]. The main land use types in each SU were used as the land use attribute of the SU.

3) *Independence Analysis of Influence Factors:* To ensure the independence of the influence factors, this study conducted a multicollinearity analysis of the nine influence factors and calculated the correlation coefficient between the factors. The results are listed in Table II. The absolute value of the correlation coefficient reflects the correlation between factors. A strong correlation between factors exists when the value is greater than 0.5. As shown in Table II, the absolute value of the correlation

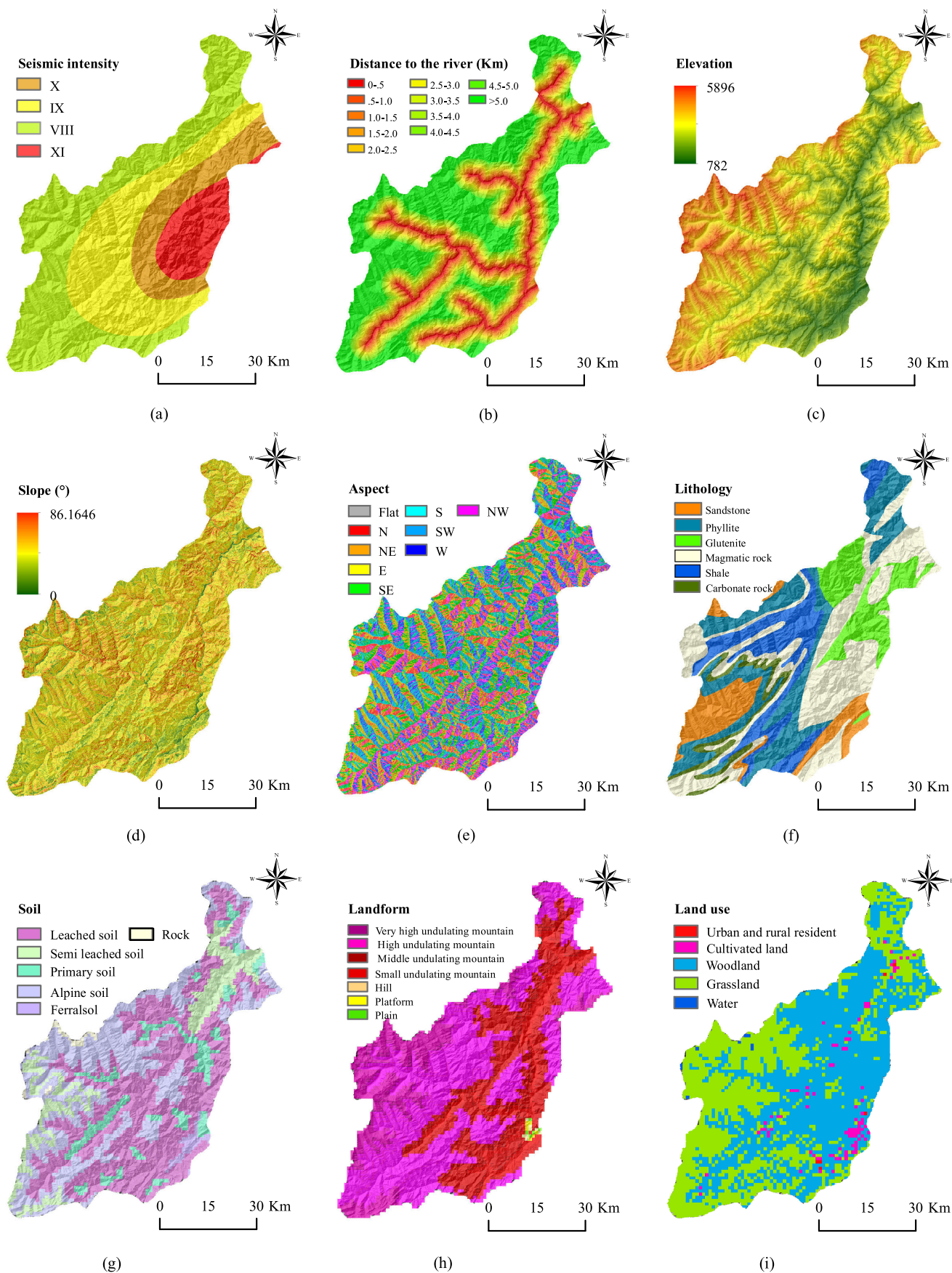


Fig. 6. Influence factor maps of the seismic landslide.

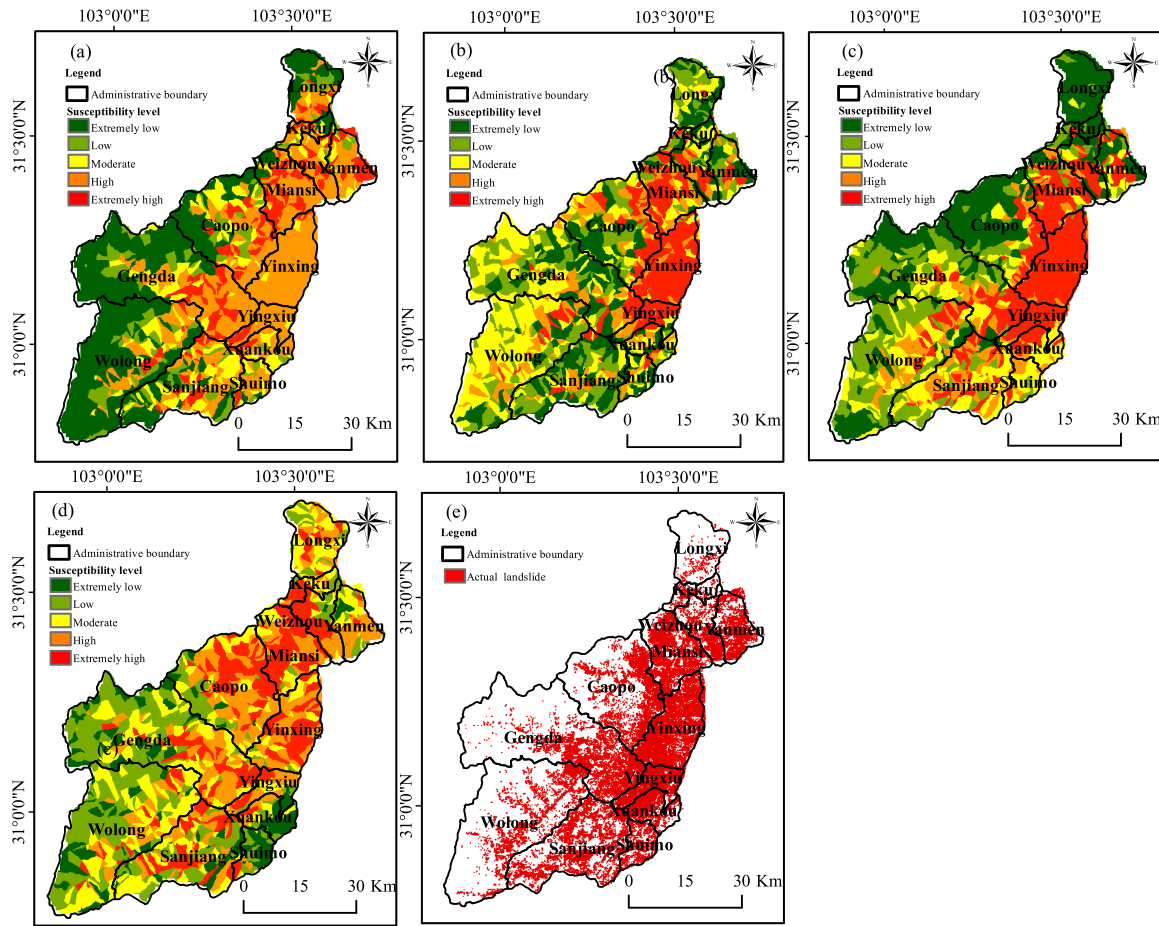


Fig. 7. Landslide susceptibility maps using SVM and the OCSVM model in Wenchuan: SVM model based on the (a) first, (b) second, and (c) third sample selection methods, (d) OCSVM model based on a single-class sample, and (e) actual landslide distribution.

among elevation, river, and landform was greater than 0.5 (0.66, 0.79, and 0.65, respectively). Hence, a strong correlation exists among the three influence factors. Compared with elevation and landform, river had a more obvious promoting effect on the landslide [17]. Therefore, the elevation and landform factors were removed in this study to ensure relative independence between the selected influence factors. In the end, seven factors (earthquake intensity, distance to the river, slope, aspect, lithology, soil, and land use) were adopted as the influence factors of the landslide susceptibility model.

C. One Class Classifier

In this study, OCSVM was used as a mathematical model for evaluating the susceptibility of seismic landslides. The model maps the sample from low- to high-dimension space by using the kernel function and finds the optimal hyperplane between the sample and origin in the high-dimension space [42]. For example, the distance from the sample to the hyperplane represents the similarity of the sample belonging to a certain category. The decision function of the OCSVM model can be expressed as follows:

$$f(x) = \text{sign}((\omega \cdot \Phi(x)) - \rho) \quad (2)$$

where $\Phi(\cdot)$ represents the sample feature space, ω and ρ denote the weight of the support vector and bias, respectively. The decision function can be transformed into a quadratic programming equation as follows:

$$\begin{aligned} \min & \frac{1}{2} \|\omega\|^2 + \frac{1}{vN} \sum_{i=1}^N \xi_i - \rho \\ \text{s.t.} & (\omega \cdot \Phi(x_i)) \geq \rho - \xi_i \quad \xi_i \geq 0 \end{aligned} \quad (3)$$

where ξ_i is the slack variable and $v \in (0, 1)$ is used to control the proportion of the support vector in the training samples. By introducing the kernel function, this problem can be transformed into a dual form as follows:

$$\begin{aligned} \min_a & \frac{1}{2} \sum_{i=1}^N \sum_{j=1}^N a_i a_j k(x_i, x_j) \\ \text{s.t.} & 0 \leq a_i \leq \frac{1}{vN} \quad \sum_{i=1}^N a_i = 1 \end{aligned} \quad (4)$$

where $k(\cdot)$ represents the kernel function, $\rho = \sum_{i=1}^N a_i K(x_i, x_j)$ denotes the bias, and ω refers to the weight of the support vector. In this study, the OCSVM model

TABLE III
PERCENTAGE DISTRIBUTION OF SEISMIC LANDSLIDES IN THE LANDSLIDE SUSCEPTIBILITY MAP

Susceptibility level	Area/km ²	Area percent (%)	Seismic landslide/km ²	Landslide percent	Density
SVM model based on the first sample selection method					
Extremely low	1346.14	0.33	11.09	0.03	0.01
Low	379.25	0.09	8.95	0.03	0.02
Moderate	451.56	0.11	26.84	0.08	0.06
High	1392.97	0.35	240.54	0.67	0.17
Extremely high	461.11	0.11	69.02	0.19	0.15
SVM model based on the second sample selection method					
Extremely low	916.15	0.23	42.10	0.12	0.05
Low	832.82	0.21	31.88	0.09	0.04
Moderate	1037.85	0.26	37.96	0.11	0.04
High	526.39	0.13	67.40	0.19	0.13
Extremely high	717.82	0.18	177.09	0.50	0.25
SVM model based on the third sample selection method					
Extremely low	1112.55	0.28	25.39	0.07	0.02
Low	791.45	0.20	21.18	0.06	0.03
Moderate	687.50	0.17	35.81	0.10	0.05
High	450.78	0.11	31.88	0.09	0.07
Extremely high	984.73	0.24	242.06	0.68	0.25
OCSVM model based on single-class samples					
Extremely low	414.25	0.10	10.96	0.03	0.03
Low	973.50	0.24	28.86	0.08	0.03
Moderate	917.23	0.23	63.06	0.18	0.07
High	908.21	0.23	128.81	0.36	0.14
Extremely high	817.84	0.20	124.76	0.35	0.15

TABLE IV
DISTRIBUTION STATISTICS OF NEW LANDSLIDE EVENTS IN LANDSLIDE SUSCEPTIBILITY

New landslide events	Latitude	Longitude	Susceptibility (SVM)	Susceptibility (OCSVM)
2009. 7. 25 (Landslide in Chediguan Bridge)	31.219	103.489	High	High
2010. 5. 30 (Landslide in Suoqiao Village)	31.496	103.645	Low	Moderate
2010. 6. 12 (Landslide in Jinbo Village)	31.220	103.412	Extremely high	High
2013. 7. 22 (Landslide in Zuwang Village)	31.296	103.443	Extremely high	Extremely high
2018. 4. 10 (Landslide in Aer Village)	31.678	103.546	Low	Moderate
2018. 7. 26 (Landslide in Minjiang Bridge)	31.475	103.575	High	High

was established using the LIBSVM package [43] by collecting landslide samples and related landslide influence factors.

IV. EXPERIMENTAL RESULTS

According to the incomplete landslide inventory obtained for the study area, the Wenchuan earthquake triggered a 170.49 km² seismic landslide in the scope of 4138 km². The proportion of the landslide was approximately 4.1%. Unlike other landslides, the seismic landslide was affected by ground motion, resulting in a seismic landslide characterized by long-distance ejection [44]; hence, the influence scope of the landslide was not limited to a single SU [45]. To ensure the reliability of the selected sample data, the slope with a proportion of more than 4.1 landslides in the SU was regarded as unstable. Through calculation, the study area was found to contain 348 unstable SUs, which were used as the primary data source of the landslide susceptibility model for analyzing landslide susceptibility.

A. Landslide Susceptibility Model Based on SVM

Compared with the traditional machine learning method, SVM has better generalization ability with the principle of structural risk minimization and is widely used in the analysis

of landslide susceptibility. Therefore, SVM, which needs to select two kinds of samples (stable and unstable slopes), was used for a comparative analysis to evaluate the reliability of the OCSVM model. This study selected the Gaussian kernel for SVM and OCSVM [19], and the most suitable parameters were determined via fourfold cross-validation. Further details on OCSVM and SVM can be found in the work of Chang and Lin [43]. To compare and analyze the influence of stable sample selection on the results of landslide susceptibility, three methods of stability sample selection were designed in this study. (1) Stable samples were selected in the landslide-free area of the complete landslide inventory. (2) Stable samples were selected in the omitting area of the incomplete landslide inventory. (3) Stable samples were selected randomly in the landslide-free area of the incomplete landslide inventory. To reflect landslide susceptibility directly, natural break classification, which is a statistical method that classifies and classifies classes according to the statistical distribution of values, was applied to divide the study area into five categories: extremely high, high, moderate, low and extremely low. The results are shown in Fig. 7(a)–(c). These figures show the obvious differences in landslide susceptibility among the three maps, indicating that stability sample selection had a significant impact on the results of SVM landslide

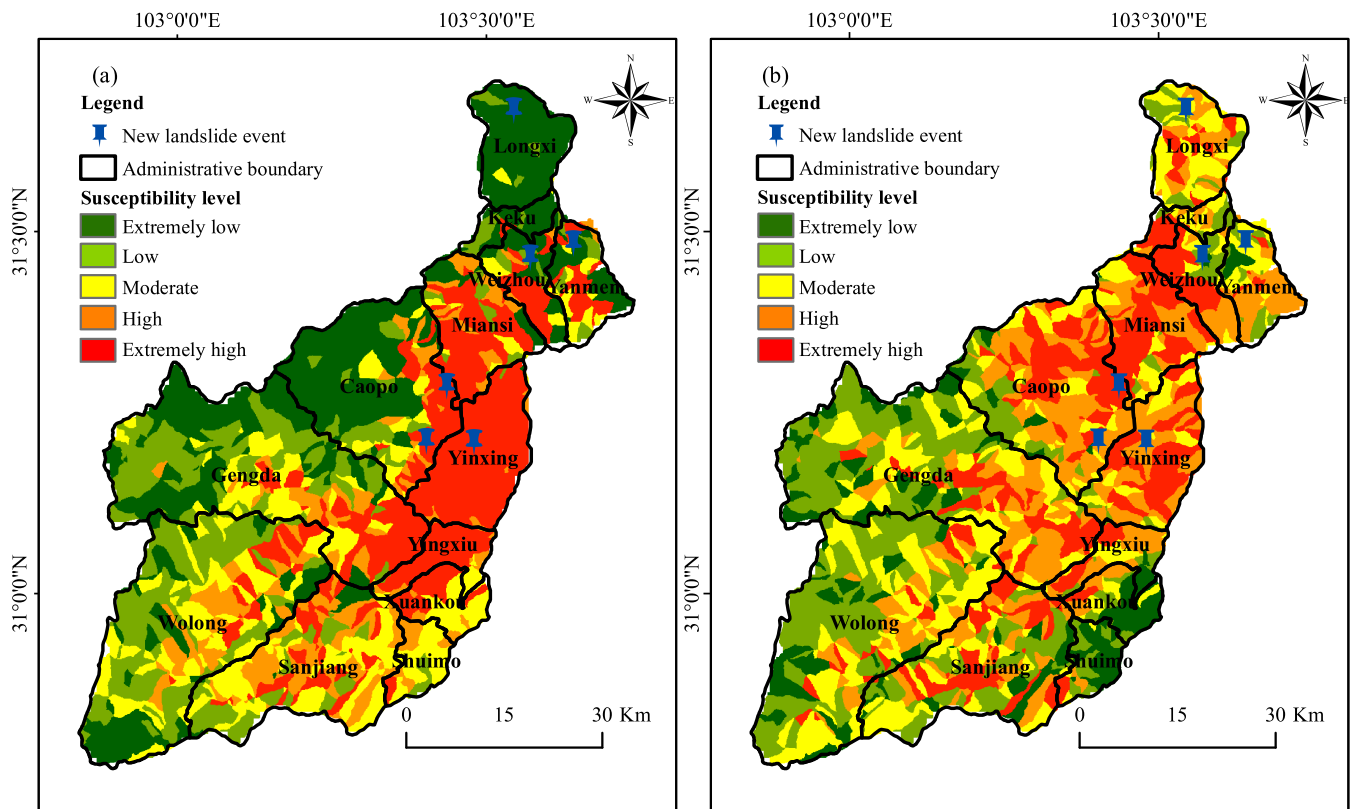


Fig. 8. Distribution of landslide susceptibility and new landslide events. (a) SVM model based on the third sample selection method. (b) OCSVM model based on a single-class sample.

susceptibility. Fig. 7(a) shows the distribution of risk areas (extremely high, high, and moderate) along the river, including the towns of Ginko, Yingxiu, Mianfan, and Weizhou, whereas the non-risk areas (low and extremely low), such as the towns of Gengda and Wolong, are mainly distributed in the southwest of Wenchuan County. This result is consistent with the distribution of landslides induced by the Wenchuan earthquake. Fig. 7(b) shows that Gengda and Wolong were classified as risk areas although these towns are minimally distributed with seismic landslides because the risk is overestimated due to the selection of stable samples in the area of omission. Fig. 7(c) shows that towns, such as Keku and Longxi, were classified as non-risk areas in the evaluation model, as a result that is different from the actual distribution of seismic landslides. In the other areas, the results of landslide susceptibility zoning were consistent with the distribution of seismic landslides.

B. Landslide Susceptibility Model Based on OCSVM

The OCSVM model only needs a single class of sample data. On the basis of the incomplete landslide inventory for the study area, a sample set was established to train the OCSVM model and obtain landslide susceptibility. Then, the study area was divided into five categories (extremely high, high, moderate, low, and extremely low) by using the natural break classification scheme. The results are illustrated in Fig. 7(d). The risk areas in the study area mainly included the towns of Ginko, Yingxiu, Mian'an, Yanmen, and Weizhou, and the non-risk areas mainly included

Shuimo and Xuankou. These findings are consistent with the actual distribution of seismic landslides.

C. Model Evaluation

The reliability of landslide susceptibility mapping was analyzed and verified using the complete landslide inventory and new landslide events in the study area.

In the model evaluation, the risk areas (extremely high, high, and moderate) in the landslide susceptibility mapping were regarded as landslide areas, and the rest (i.e., low and extremely low) were considered landslide-free areas. Therefore, more actual landslides were located in the risk areas than in the non-risk ones, indicating a higher prediction ability for the former. In this study, the exact seismic landslide location was determined by the complete landslide inventory. For the SVM model, a landslide susceptibility map was obtained via the three methods of landslide-free sample selection, and the actual landslide areas in each zone were counted. The statistical results are presented in Table III. In the first case, the model was constructed based on the complete landslide inventory. The accuracy of the model was high, and the proportion of actual landslides that developed in the risk area was 94%. In the second case, because the landslide-free samples were in the omission area of the incomplete landslide inventory, the model was constructed in the worst case. The accuracy of the model was low, and only 80% of the actual landslides were developed in the risk area. In the third case, the research focus of this study is based on the incomplete landslide

inventory. The accuracy of the model was between that in the first and second cases, and the actual landslides that developed in the risk area accounted for 87%.

Different from the SVM model, the OCSVM model only needs a single class of sample data and is thus unaffected by the selection of landslide-free samples. Therefore, this study used the incomplete landslide inventory to build landslide susceptibility mapping on the basis of the OCSVM model and counted the actual landslides in each zone. The results (Table III) showed that the real landslides that developed in the risk area accounted for 89%, which is at a high level. In conclusion, in the case of complete landslide inventory in the study area, the result of the SVM model is better than that of the OCSVM model, which is consistent with existing research. When a complete landslide inventory is difficult to obtain quickly, the OCSVM model only needs a single kind of sample data to achieve reliable landslide susceptibility mapping, which is helpful in providing a basis for emergency rescue work after an earthquake.

Landslide susceptibility is mainly used to evaluate the possibility of subsequent landslides. Therefore, new landslide events are also a valuable reference for verifying the assessment results of landslide susceptibility. Hence, six new landslide events that occurred after the Wenchuan earthquake were identified by searching for new landslides on the Internet. The locations of these landslides were determined by conducting a historical Google search of remote sensing images, as shown in Table IV. In accordance with this point of view, the SVM model constructed by the standard random sample selection method (the third sample selection method) and the OCSVM model built by a single class of samples were selected, and an overlay analysis with the new landslide event locations was conducted. The results are shown in Fig. 8(a) and (b). The statistics on landslide susceptibility corresponding to the new landslide events and analysis of the reliability of the landslide susceptibility results are presented in Table IV. For the OCSVM model, new landslide events occurred in the risk areas (extremely high, high, and moderate), whereas for the SVM model, two landslide events occurred in the non-risk areas (low and extremely low). The analysis of the distribution of new landslide events indicated that the landslide susceptibility obtained by the OCSVM model is more consistent with the actual situation, and the results are more reliable than those of SVM.

V. CONCLUSION

This study analyzed the applicability of the OCSVM model in landslide susceptibility under the condition of incomplete landslide inventory. SU was used as the mapping unit, and seven influence factors (slope, aspect, lithology, distance from the river, soil type, seismic intensity, and land use) were selected for the construction of the OCSVM model for the analysis of landslide susceptibility in Wenchuan County. Compared with the traditional SVM model, OCSVM only needs a single kind of sample data. It has minimal dependence on the complete landslide inventory and exerts little influence on landslide-free sample selection. OCSVM showed the advantages of stable

precision and reliable prediction results. In conclusion, under the condition that obtaining a complete landslide inventory after an earthquake is difficult, the proposed method can quickly obtain a landslide susceptibility map and provide essential guidance for emergency response, rescue, and subsequent land use planning after earthquakes. The influence of the incomplete level on landslide mapping accuracies of different methods would be an interesting research direction in future work.

ACKNOWLEDGMENT

The authors would like to thank the anonymous reviewers for their constructive and valuable comments that significantly contributed to improving the article.

REFERENCES

- [1] C. Xu, X. Xu, X. Yao, and F. Dai, "Three (nearly) complete inventories of landslides triggered by the May 12, 2008 Wenchuan mw 7.9 earthquake of China and their spatial distribution statistical analysis," *Landslides*, vol. 11, no. 3, pp. 441–461, 2014.
- [2] P. Reichenbach, M. Rossi, B. D. Malamud, M. Mihir, and F. Guzzetti, "A review of statistically-based landslide susceptibility models," *Earth-Sci. Rev.*, vol. 180, pp. 60–91, 2018.
- [3] R. W. Jibson, E. L. Harp, and J. A. Michael, "A method for producing digital probabilistic seismic landslide hazard maps," *Eng. Geol.*, vol. 58, no. 3/4, pp. 271–289, 2000.
- [4] M. Carro, M. De Amicis, L. Luzi, and S. Marzorati, "The application of predictive modeling techniques to landslides induced by earthquakes: The case study of the 26 September 1997 Umbria-Marche earthquake (Italy)," *Eng. Geol.*, vol. 69, no. 1/2, pp. 139–159, 2003.
- [5] K.-L. Wang and M.-L. Lin, "Development of shallow seismic landslide potential map based on Newmark's displacement: The case study of Chi-Chi earthquake, Taiwan," *Environmental Earth Sci.*, vol. 60, no. 4, pp. 775–785, 2010.
- [6] H.-Y. Tsai, C.-C. Tsai, and W.-C. Chang, "Slope unit-based approach for assessing regional seismic landslide displacement for deep and shallow failure," *Eng. Geol.*, vol. 248, pp. 124–139, 2019.
- [7] Y. Wang, C. Song, Q. Lin, and J. Li, "Occurrence probability assessment of earthquake-triggered landslides with Newmark displacement values and logistic regression: The Wenchuan earthquake, China," *Geomorphology*, vol. 258, pp. 108–119, 2016.
- [8] K. Jin, L. Yao, Q. Cheng, and A. Xing, "Seismic landslides hazard zoning based on the modified Newmark model: A case study from the Lushan earthquake, China," *Natural Hazards*, vol. 99, no. 1, pp. 493–509, 2019.
- [9] S. Ma and C. Xu, "Assessment of co-seismic landslide hazard using the Newmark model and statistical analyses: A case study of the 2013 Lushan, China, Mw6.6 earthquake," *Natural Hazards*, vol. 96, no. 1, pp. 389–412, 2019.
- [10] S. F. Gallen, M. K. Clark, J. W. Godt, K. Roback, and N. A. Niemi, "Application and evaluation of a rapid response earthquake-triggered landslide model to the 25 April 2015 Mw7.8 Gorkha earthquake, Nepal," *Tectonophysics*, vol. 714, pp. 173–187, 2017.
- [11] M. Shinoda, Y. Miyata, U. Kurokawa, and K. Kondo, "Regional landslide susceptibility following the 2016 Kumamoto earthquake using back-calculated geomaterial strength parameters," *Landslides*, vol. 16, no. 8, pp. 1497–1516, 2019.
- [12] J. Jia-Liang, W. Yin, G. Dan, Y. Ren-Mao, and Y. Xiao-Yan, "New evaluation models of Newmark displacement for Southwest China," *Bull. Seismological Soc. Amer.*, vol. 108, no. 4, pp. 2221–2236, 2018.
- [13] D. Dreyfus, E. M. Rathje, and R. W. Jibson, "The influence of different simplified sliding-block models and input parameters on regional predictions of seismic landslides triggered by the Northridge earthquake," *Eng. Geol.*, vol. 163, pp. 41–54, 2013.
- [14] Y. Yi, Z. Zhang, W. Zhang, Q. Xu, C. Deng, and Q. Li, "Gis-based earthquake-triggered-landslide susceptibility mapping with an integrated weighted index model in Jiuzhaigou region of Sichuan Province, China," *Natural Hazards Earth Syst. Sci.*, vol. 19, no. 9, pp. 1973–1988, 2019.
- [15] S. Mondal and S. Mandal, "Landslide susceptibility mapping of Darjeeling Himalaya, India using index of entropy (IOE) model," *Appl. Geomatics*, vol. 11, no. 2, pp. 129–146, 2019.

- [16] P. Kayastha, M. R. Dhital, and F. De Smedt, "Landslide susceptibility mapping using the weight of evidence method in the Tinau watershed, Nepal," *Natural Hazards*, vol. 63, no. 2, pp. 479–498, 2012.
- [17] C. Xu *et al.*, "Application of an incomplete landslide inventory, logistic regression model and its validation for landslide susceptibility mapping related to the May 12, 2008 Wenchuan earthquake of China," *Natural Hazards*, vol. 68, no. 2, pp. 883–900, 2013.
- [18] A. A. Shahri, J. Spross, F. Johansson, and S. Larsson, "Landslide susceptibility hazard map in Southwest Sweden using artificial neural network," *Catena*, vol. 183, 2019, Art. no. 104225.
- [19] W. Chen, H. Chai, Z. Zhao, Q. Wang, and H. Hong, "Landslide susceptibility mapping based on GIS and support vector machine models for the Qianyang County, China," *Environmental Earth Sci.*, vol. 75, no. 6, 2016, Art. no. 474.
- [20] H. R. Pourghasemi, A. G. Jirandeh, B. Pradhan, C. Xu, and C. Gokceoglu, "Landslide susceptibility mapping using support vector machine and GIS at the Golestan Province, Iran," *J. Earth Syst. Sci.*, vol. 122, no. 2, pp. 349–369, 2013.
- [21] J.-C. Kim, S. Lee, H.-S. Jung, and S. Lee, "Landslide susceptibility mapping using random forest and boosted tree models in Pyeong-Chang, Korea," *Geocarto Int.*, vol. 33, no. 9, pp. 1000–1015, 2018.
- [22] B. Pradhan, "A comparative study on the predictive ability of the decision tree, support vector machine and neuro-fuzzy models in landslide susceptibility mapping using GIS," *Comput. Geosci.*, vol. 51, pp. 350–365, 2013.
- [23] B. T. Pham, B. Pradhan, D. T. Bui, I. Prakash, and M. Dholakia, "A comparative study of different machine learning methods for landslide susceptibility assessment: A case study of Uttarakhand area (India)," *Environmental Model. Softw.*, vol. 84, pp. 240–250, 2016.
- [24] H. Hong, B. Pradhan, D. T. Bui, C. Xu, A. M. Youssef, and W. Chen, "Comparison of four kernel functions used in support vector machines for landslide susceptibility mapping: A case study at Suichuan area (China)," *Geomatics, Natural Hazards Risk*, vol. 8, no. 2, pp. 544–569, 2017.
- [25] J. Zêzere, S. Pereira, R. Melo, S. Oliveira, and R. A. Garcia, "Mapping landslide susceptibility using data-driven methods," *Sci. Total Environ.*, vol. 589, pp. 250–267, 2017.
- [26] F. Huang, K. Yin, J. Huang, L. Gui, and P. Wang, "Landslide susceptibility mapping based on self-organizing-map network and extreme learning machine," *Eng. Geol.*, vol. 223, pp. 11–22, 2017.
- [27] T. Gorum *et al.*, "Distribution pattern of earthquake-induced landslides triggered by the 12 May 2008 Wenchuan earthquake," *Geomorphology*, vol. 133, no. 3–4, pp. 152–167, 2011.
- [28] X. Fan *et al.*, "Coseismic landslides triggered by the 8th August 2017 MS 7.0 Jiuzhaigou earthquake (Sichuan, China): Factors controlling their spatial distribution and implications for the seismogenic blind fault identification," *Landslides*, vol. 15, no. 5, pp. 967–983, 2018.
- [29] Z. Li, W. Shi, S. W. Myint, P. Lu, and Q. Wang, "Semi-automated landslide inventory mapping from bitemporal aerial photographs using change detection and level set method," *Remote Sens. Environ.*, vol. 175, pp. 215–230, 2016.
- [30] Z. Y. Lv, W. Shi, X. Zhang, and J. A. Benediktsson, "Landslide inventory mapping from bitemporal high-resolution remote sensing images using change detection and multiscale segmentation," *IEEE J. Sel. Topics Appl. Earth Observ. Remote Sens.*, vol. 11, no. 5, pp. 1520–1532, May 2018.
- [31] Z. Y. Lv, T. F. Liu, P. Zhang, J. A. Benediktsson, T. Lei, and X. Zhang, "Novel adaptive histogram trend similarity approach for land cover change detection by using bitemporal very-high-resolution remote sensing images," *IEEE Trans. Geosci. Remote Sens.*, vol. 57, no. 12, pp. 9554–9574, Dec. 2019.
- [32] F. Chen, B. Yu, and B. Li, "A practical trial of landslide detection from single-temporal Landsat8 images using contour-based proposals and random forest: A case study of national Nepal," *Landslides*, vol. 15, no. 3, pp. 453–464, 2018.
- [33] T. R. Martha, N. Kerle, C. J. Van Westen, V. Jetten, and K. V. Kumar, "Object-oriented analysis of multi-temporal panchromatic images for creation of historical landslide inventories," *ISPRS J. Photogrammetry Remote Sens.*, vol. 67, pp. 105–119, 2012.
- [34] R. N. Keyport, T. Oommen, T. R. Martha, K. Sajinkumar, and J. S. Gierke, "A comparative analysis of pixel-and object-based detection of landslides from very high-resolution images," *Int. J. Appl. Earth Observ. Geoinf.*, vol. 64, pp. 1–11, 2018.
- [35] A. Si *et al.*, "Regional landslide identification based on susceptibility analysis and change detection," *ISPRS Int. J. Geo-Inf.*, vol. 7, no. 10, pp. 1–27, 2018.
- [36] W. Zhao, A. Li, X. Nan, Z. Zhang, and G. Lei, "Postearthquake landslides mapping from Landsat-8 data for the 2015 Nepal earthquake using a pixel-based change detection method," *IEEE J. Sel. Topics Appl. Earth Observ. Remote Sens.*, vol. 10, no. 5, pp. 1758–1768, May 2017.
- [37] R. N. Ramos-Bernal, R. Vázquez-Jiménez, R. Romero-Calcerrada, P. Arrogante-Funes, and C. J. Novillo, "Evaluation of unsupervised change detection methods applied to landslide inventory mapping using Aster imagery," *Remote Sens.*, vol. 10, no. 12, pp. 1–24, 2018.
- [38] L. Nahayo, E. Kalisa, A. Maniragaba, and F. X. Nshimiyimana, "Comparison of analytical hierarchy process and certain factor models in landslide susceptibility mapping in Rwanda," *Model. Earth Syst. Environ.*, vol. 5, pp. 885–895, 2019.
- [39] Q. Ba, Y. Chen, S. Deng, J. Yang, and H. Li, "A comparison of slope units and grid cells as mapping units for landslide susceptibility assessment," *Earth Sci. Informat.*, vol. 11, no. 3, pp. 373–388, 2018.
- [40] J. Broeckx, M. Vanmaercke, R. Duchateau, and J. Poesen, "A data-based landslide susceptibility map of Africa," *Earth-Sci. Rev.*, vol. 185, pp. 102–121, 2018.
- [41] F. Dai, C. Xu, X. Yao, L. Xu, X. Tu, and Q. Gong, "Spatial distribution of landslides triggered by the 2008 MS 8.0 Wenchuan earthquake, China," *J. Asian Earth Sci.*, vol. 40, no. 4, pp. 883–895, 2011.
- [42] B. Schölkopf, R. C. Williamson, A. J. Smola, J. Shawe-Taylor, and J. C. Platt, "Support vector method for novelty detection," in *Proc. Adv. Neural Inf. Process. Syst.*, 2000, pp. 582–588.
- [43] C.-C. Chang and C.-J. Lin, "LIBSVM: A library for support vector machines," *ACM Trans. Intell. Syst. Technol.*, vol. 2, no. 3, pp. 1–27, 2011.
- [44] R. Q. Huang and W. L. Li, "Analysis of the geo-hazards triggered by the 12 May 2008 Wenchuan earthquake, China," *Bull. Eng. Geol. Environ.*, vol. 68, no. 3, pp. 363–371, 2009.
- [45] A. Erener and H. Düzgün, "Landslide susceptibility assessment: What are the effects of mapping unit and mapping method?" *Environmental Earth Sci.*, vol. 66, no. 3, pp. 859–877, 2012.



Shuai Chen received the B.S. degree from the Longyan University, China, in 2012, and the M.S. degree from the Changsha University of Science & Technology, China. He is currently working toward the Ph.D. degree in photogrammetry and remote sensing from Central South University, China.

His research interests include landslide extraction, landslide susceptibility mapping, and landslide risk analysis.



Zelang Miao (Member, IEEE) received the B.S. degree in surveying engineering and the M.S. degree in geodesy and surveying engineering from the China University of Mining and Technology, Xuzhou, China, in 2009 and 2014, respectively, and the Ph.D. degree in satellite image processing from The Hong Kong Polytechnic University, Hong Kong, in 2016.

He was a visiting Ph.D. Student at the Department of Industrial and Information Engineering, University of Pavia, Pavia, Italy, in 2015. He is currently an Associate Professor with the School of Geoscience and Info-Physics, Central South University, Changsha, China. He has authored or co-authored over 30 papers on international and peer-reviewed scientific journals. His research interests include pattern recognition, land cover and land use mapping, and global/regional urbanization.

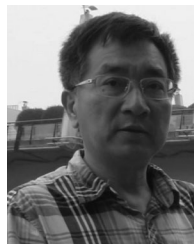
Dr. Miao serves as a referee for IEEE Transactions on Geoscience and Remote Sensing, and IEEE Journal of Selected Topics in Remote Sensing Applications, Remote Sensing.



Lixin Wu received the B.S. degree in mining survey from the China University of Mining and Technology, Xuzhou, China, in 1988, and the M.S. and Ph.D. degrees in geomatics from the China University of Mining and Technology, Beijing, China, in 1991 and 1997, respectively.

He is currently a Professor with the School of Geoscience and Info-Physics, Central South University. His research interests include geohazards synergic observation, remote sensing rock mechanic, and geospatial informatics.

Dr. Wu is currently a member of the Infrastructure Implementation Board of Group on Earth Observation, the Vice Chairman of Space Observation Committee of China Seismology Society, and the Editor-in-Chief of the Journal of Geography and Geo-Information Science (Chinese).



Yueguang He received the B.S. degree in surveying engineering and M.S. and Ph.D. degrees in geodesy and surveying engineering from Central South University, China, in 1987, 1993, and 2003, respectively.

He is currently a Professor with Changsha University of Science Technology, China. His research interests include geohazards synergic observation and deformation monitoring.